Connection of segmented intensity data measured with a multiple-detector system for powder diffractometry

T. Ida

Connection of segmented intensity data measured with a multiple-detector system for powder diffractometry

T. Ida

Ceramics Research Laboratory, Nagoya Institute of Technology, Asahigaoka, Tajimi, 507-0071 Japan. Correspondence e-mail: ida.takashi@nitech.ac.jp

A Fourier method to connect segmented intensity data measured with a multiple-detector system (MDS) for powder diffractometry has been developed. Differences in sensitivity, slight shifts in peak positions and asymmetric instrumental broadening for different detectors are simultaneously adjusted by a Fourier-based deconvolution/convolution method. The Fourier transform of the adjustment function is evaluated as the ratio of the Fourier transforms of the intensity data sets in the overlapped region measured with the adjacent detectors. Even and odd polynomial functions with maximum order of 10 are separately fitted to the real and imaginary parts of the experimentally evaluated Fourier-transformed adjustment by a least-squares method applying an appropriate weighting for the Fourier-transformed data. The complex of the optimized polynomials is used to adjust the data measured with a detector in order to connect them with the data measured with an adjacent detector. The method is applied to connect the powder diffraction data of ZnO powder measured with the MDS on beamline $BL4B_2$ at the Photon Factory in Tsukuba. Slight differences in line width, asymmetry and sharpness detected in the observed diffraction peak profiles measured with the different detectors have successfully been removed by the Fourier-based adjustment procedures.

1. Introduction

A multiple-detector system (MDS) for powder X-ray diffraction measurement has been utilized on beamline $BL4B_2$ at the Photon Factory in Tsukuba (Toraya *et al.*, 1996). High-resolution diffraction intensity data in the range 0–155° with typical step intervals of 0.004° or 0.005° in 2Θ can be collected within about 10 h, which is made possible by the enhanced efficiency of data acquisition owing to the multiplication of the detection system. When the 2Θ axis of the MDS is scanned over an angular range of 0–30°, six sets of detection systems, attached radially at intervals of 25° to the 2Θ axis, simultaneously provide diffraction intensity data in the ranges 0–30°, 25–55°, 50–80°, 75–105°, 100–130° and 125–155° in 2Θ. A similar design of a powder diffractometer for beamline B2 at HASYLAB/DESY in Hamburg has been reported by Kaps *et al.* (1999). Multiple-detector powder diffractometers based on a single-axis multiple-analyser design (Hodeau *et al.*, 1998) are also in operation at ESRF in Grenoble, and other facilities.

The diffraction intensity profiles measured with different detectors do not exactly coincide with one another, because the difference in intrinsic sensitivity of the detectors, the relative intensity of stray light, and small deviations of the analyser tilt angle from the strictly aligned condition (Ida *et al.*, 2001) can all affect the observed diffraction intensity profile. Slightly different characteristics of the detectors should be taken into account when treating the segmented intensity data measured with the MDS, especially for the application to the detailed analysis of peak profiles aimed at the evaluation of microstructure parameters of polycrystalline samples.

In principle, the different instrumental functions of detectors can be explicitly taken into account by applying convoluted peak profile functions, as has been suggested in our previous report (Ida *et al.*, 2001). However, it would be more convenient if the slight deviation in the instrumental function of a detector could be adjusted and a series of combined data were made available by simply merging the segments of the adjusted intensity data.

Toraya *et al.* (1996) have suggested that small disagreements in peak position and intensity for the same reflections observed with the two adjacent detectors can be adjusted by a least-squares method applied to the data in the overlapping regions. Background, sensitivity and shift of the angle can be adjusted by linear transformations for the data of 2Θ and intensity.

However, the instrumental peak broadenings caused by slight misalignment of the analyser crystals are also likely to vary for different detector systems (Ida *et al.*, 2001), which cannot be adjusted by linear transformations of data.

In this paper, a new method is proposed for adjusting slight deviations of the instrumental functions to connect partially

overlapped segmented intensity data measured with a multiple-detector system. The method is applied to the diffraction intensity data of a standard ZnO powder sample (NIST SRM674) measured with the MDS at the Photon Factory, and the validity of the method is examined by detailed analyses of the observed and adjusted diffraction peak profiles.

2. Method

2.1. Concept of Fourier-based adjustment

It is assumed that two segments of intensity profiles, $y_1 = g_1(x)$ over the range $x_{11} \leq x \leq x_{12}$ and $y_2 = g_2(x)$ over the range $x_{21} \leq x \leq x_{22}$, are measured with detectors with different instrumental functions $w_1(x)$ and $w_2(x)$, respectively, where the overlapped range is given by $x_{21} \leq x \leq x_{12}$. The intrinsic (instrument-free) intensity profile is assumed to be $y = f(x)$. The convolution relations are expressed by the following equations:

$$g_1(x) = f(x) * w_1(x) \quad (x_{11} \leq x \leq x_{12}) \qquad (1)$$

and

$$g_2(x) = f(x) * w_2(x) \quad (x_{21} \leq x \leq x_{22}), \qquad (2)$$

where $f(x) * w(x)$ is the convolution of $f(x)$ and $w(x)$, defined by

$$f(x) * w(x) \equiv \int_{-\infty}^{\infty} f(x - y)w(y)\, dy. \qquad (3)$$

The purpose of the method is to modify the second set of intensity data $y_2 = g_2(x)$, as if they were measured with a detector with the same instrumental function as the first detector, $w_1(x)$. It can be achieved, in principle, by deconvolution with $w_2(x)$ followed by convolution of $w_1(x)$.

Even if the exact formulae of the instrumental functions $w_1(x)$ and $w_2(x)$ is unknown, an empirical deconvolution/ convolution method can be applied by the following procedures, similarly to the method of Stokes (1948).

If the widths of the instrumental functions are sufficiently narrower than the overlapped range, the Fourier transform of the instrumental adjustment function $W_{1/2}(\xi)$ can be related to the experimental data by the following equation:

$$W_{1/2}(\xi) = G_{o1}(\xi)/G_{o2}(\xi) \qquad (4)$$

where $G_{o1}(\xi)$ and $G_{o2}(\xi)$ are the Fourier transforms of the intensity data within the overlapped region, i.e.

$$G_{o1}(\xi) = \int_{x_{21}}^{x_{12}} g_1(x) \exp(2\pi i \xi x)\, dx \qquad (5)$$

and

$$G_{o2}(\xi) = \int_{x_{21}}^{x_{12}} g_2(x) \exp(2\pi i \xi x)\, dx. \qquad (6)$$

The intensity data y_2 should be adjusted to $y_{2'} = g_{2'}(x)$, by the following equation:

$$g_{2'}(x) = \int_{-\infty}^{\infty} W_{1/2}(\xi) G_2(\xi) \exp(-2\pi i \xi x)\, d\xi, \qquad (7)$$

where $G_2(\xi)$ is calculated for the whole region measured with the second detector by

$$G_2(\xi) = \int_{x_{21}}^{x_{22}} g_2(x) \exp(2\pi i \xi x)\, dx. \qquad (8)$$

In a discrete formula, the adjusted data $\{(y_{2'})_j\}$ are calculated from the source intensity data $\{(y_2)_j\}$ by the following equation:

$$(y_{2'})_j = N^{-1} \sum_k (W_{1/2})_k (G_2)_k \exp(-2\pi i k j/N), \qquad (9)$$

where $\{(W_{1/2})_k\}$ is the discrete Fourier-transformed adjustment function, and $\{(G_2)_k\}$ is the discrete Fourier transform of the second intensity data set given by

$$(G_2)_k = \sum_j (y_2)_j \exp(2\pi i k j/N). \qquad (10)$$

The discrete Fourier-transformed adjustment $\{(W_{1/2})_k\}$ to be applied to the N-point segmented data $\{(y_2)_j\}$ is evaluated by a smoothing interpolation from the experimental values $\{(W_{o,1/2})_{k'}\}$ evaluated from the overlapping n-point intensity data $\{(y_1)_{j'}\}$ and $\{(y_2)_{j'}\}$. Details about the methods for smoothing interpolation will be described in the following sections. The discrete formula of the adjustment function $\{(W_{1/2})_k\}$ for the whole data segment is connected with the experimental evaluation of the adjustment $\{(W_{o,1/2})_{k'}\}$ through the continuous formula $W_{1/2}(\xi)$ by the following equations:

$$(W_{1/2})_k = W_{1/2}(k/N\Delta x), \qquad (11)$$

and

$$(W_{o,1/2})_{k'} \simeq W_{1/2}(k'/n\Delta x), \qquad (12)$$

where Δx is the step interval of the source data. The experimental evaluation of $\{(W_{o,1/2})_{k'}\}$ is given by

$$(W_{o,1/2})_{k'} = (G_{o1})_{k'}/(G_{o2})_{k'}, \qquad (13)$$

where

$$(G_{o1})_{k'} = \sum_{j'} (y_1)_{j'} \exp(2\pi i k' j'/n), \qquad (14)$$

and

$$(G'_{o2})_{k'} = \sum_{j'} (y_2)_{j'} \exp(2\pi i k' j'/n). \qquad (15)$$

2.2. Preliminary corrections

It is most unlikely that the experimentally evaluated adjustment function $\{(W_{o,1/2})_{k'}\}$ would be smooth enough, because it can be heavily affected by statistical errors included in the source data. Smoothing of the adjustment function $W_{1/2}(\xi)$ is necessary to avoid increases of noise in the adjusted data through the Fourier treatment.

We can imagine that the Fourier-transformed adjustment function could be fitted by a polynomial of ξ when the background intensity is proportional to the peak intensity and the

peak shift of the instrumental function $w_2(x)$ from $w_1(x)$ is sufficiently small. For example, the adjustment function $W_{1/2}(\xi)$ will be constant if the instrumental function $w_2(x)$ is exactly proportional to $w_1(x)$, and it will be only slightly deviated from a constant function when the difference between the functions $w_2(x)$ and $w_1(x)$ is small in shape.

In contrast, it would be difficult to model a large shift in the peak position or additional intensity background by a polynomial fit applied to the Fourier-transformed adjustment function, because the constant shift (δ) corresponds to multiplication of a vibrating function $\exp(2\pi i \xi \delta)$, and the additional background corresponds to addition of a term multiplied by the Dirac delta function in the Fourier form, both of which cannot be fitted with low-order polynomials of ξ.

Therefore, it is preferred that coarse corrections of data for shift and background are conducted before the deconvolution/convolution treatment proposed in the preceding section. Fine corrections for the residual background and shift after the preliminary corrections can be included in the Fourier-based adjustment function $W_{1/2}(\xi)$, if polynomials of sufficiently high order are used.

2.2.1. Preliminary correction of shift by maximizing correlation. Evaluation of shift on the abscissa is achieved by finding the maximum of the mutual correlation function of the overlapping data, defined by

$$\mathrm{corr}(x) = \int_{x_{21}+\zeta}^{x_{12}-\zeta} g_1(z)g_2(z+x)\,\mathrm{d}z, \tag{16}$$

with

$$-\zeta < x < \zeta \tag{17}$$

where ζ is the margin to keep the variable of the integrand within the defined data range. For example, ζ can be set to $0.1°$, and $\mathrm{corr}(x)$ should be evaluated only for the range $-0.1 < x < 0.1°$, when the possible angular shift is known to be smaller than $0.1°$, as is expected for the MDS on BL4B$_2$ at the Photon Factory.

The discrete formula for the correlation $\{C_l\}$ is given by

$$C_l = \sum_{j'} y_{1j'} y_{2,j'+l}, \tag{18}$$

where the summation is calculated over the range defined by

$$x_{21} + \zeta < x_{j'} < x_{12} - \zeta \tag{19}$$

for the abscissa $x_{j'}$ at point j'.

The following formula for a Lorentzian model function can be used to determine the peak position of the correlation:

$$p(x;\, b, S, x_0, w) = b + S f_{\mathrm{Lor}}(x - x_0;\, w) \tag{20}$$

and

$$f_{\mathrm{Lor}}(x;\, w) = (\pi w)^{-1}(1 + x^2/w^2)^{-1}, \tag{21}$$

where b is the background, S the intensity, x_0 the peak position and w the half-width at half-maximum of the peak.

The shift-corrected intensity data $\{(y_{2s})_j\}$ are created by sampling intensity values at the points shifted by x_0 from the intensity curve calculated by a cubic spline interpolation for $\{(y_2)_j\}$.

2.2.2. Correction of additional background. The difference of background contributions in the two sets of intensity data $\{(y_1)_j\}$ and $\{(y_{2s})_j\}$ can be estimated by evaluating the intersection of the experimental dependence of $\{(y_{2s})_{j'}\}$ on $\{(y_1)_{j'}\}$ at $(y_1)_{j'} \to 0$ within the overlapping region. It can be achieved by a simple fitting method with a linear function, which corresponds to the approximation

$$(y_{2s})_{j'} \simeq B + A(y_1)_{j'}, \tag{22}$$

where A and B are the parameters to be optimized by a least-squares method. The different contributions of the additional part of background are simply corrected by subtracting the optimized value of B from the shift-corrected intensity data $\{(y_{2s})_j\}$. The intensity data after the preliminary corrections of shift and background $\{(y_{2p})_j\}$ are then given by

$$(y_{2p})_j = (y_{2s})_j - B. \tag{23}$$

2.3. Model for Fourier adjustment function

In general, the characteristic features of the instrumental functions $w_1(x)$ and $w_2(x)$ are mainly included in low-ξ data in the Fourier transformed form, while high-ξ data are heavily affected by statistical uncertainties.

Therefore, appropriate weighting of the data is the key for modelling the Fourier adjustment function $W_{1/2}(\xi)$ by an optimization method, thereby attaching greater importance to the low-ξ data than high-ξ data.

2.3.1. Weighting scheme. It is assumed that the errors in the source intensity data, $\{(y_1)_{j'}\}$ and $\{(y_{2p})_{j'}\}$, are independent and known to be $\{(\varepsilon_1)_{j'}\}$ and $\{(\varepsilon_{2p})_{j'}\}$, respectively. Neglecting the mutual correlations in the Fourier transforms of the intensity data, the variances of the Fourier transforms are approximated by

$$\langle |(G_{o1})_{k'} - \langle (G_{o1})_{k'}\rangle|^2 \rangle \simeq \sum_{j'}(\varepsilon_1)_{j'}^2 \tag{24}$$

and

$$\langle |(G_{o2})_{k'} - \langle (G_{o2})_{k'}\rangle|^2 \rangle \simeq \sum_{j'}(\varepsilon_{2p})_{j'}^2. \tag{25}$$

Then, the variance of the Fourier adjustment function $\{(W_{o,1/2})_{k'}\}$ is approximately given by

$$\begin{aligned} \sigma_{k'}^2 &= \langle |(W_{o,1/2})_{k'} - \langle (W_{o,1/2})_{k'}\rangle|^2 \rangle \\ &\simeq \langle |(G_{o2})_{k'}|^2 \rangle^{-1} \sum_{j'}(\varepsilon_1)_{j'}^2 \\ &\quad + \langle |(G_{o1})_{k'}|^2 \rangle \langle |(G_{o2})_{k'}|^2 \rangle^{-2} \sum_{j'}(\varepsilon_{2p})_{j'}^2, \end{aligned} \tag{26}$$

on the assumption that the errors are small as compared with the absolute values of the Fourier transforms.

It should be noted that the variances estimated by equation (26) are roughly proportional to the inverse squared absolute values of the Fourier transforms, $(G_{o1})_{k'}$ and $(G_{o2})_{k'}$. This means that the ordinary weighting scheme for least-squares

optimization, multiplying each term by $\sigma_{k'}^{-2}$, certainly attaches heavier weights to the low-ξ data.

2.3.2. Polynomial fit. The real and imaginary parts of the Fourier adjustment are separately fitted with polynomials of $\xi = k'/n\Delta x$, minimizing

$$S_R = \sum_{k'} \sigma_{k'}^{-2} \left[\mathrm{Re}(W_{o,1/2})_{k'} - f_{\mathrm{poly,R}}(k'/n\Delta x) \right]^2 \quad (27)$$

and

$$S_I = \sum_{k'} \sigma_{k'}^{-2} \left[\mathrm{Im}(W_{o,1/2})_{k'} - f_{\mathrm{poly,I}}(k'/n\Delta x) \right]^2, \quad (28)$$

where $f_{\mathrm{poly,R}}(\xi)$ and $f_{\mathrm{poly,I}}(\xi)$ are even and odd polynomials of ξ, respectively.

The model for the Fourier adjustment function is given by

$$W_{1/2}(\xi) = f_{\mathrm{poly,R}}(\xi) + if_{\mathrm{poly,I}}(\xi). \quad (29)$$

2.4. Estimation of errors

Even though it is difficult to evaluate the exact values of errors in the data modified by a Fourier-based treatment, a method for evaluating a rough indication of the errors from the source error data $\{(\varepsilon_2)_j\}$ is available (Ida & Toraya, 2002). Note that the data $\{(y_{2'})_j\}$ are calculated by the inverse Fourier transform of the product of the Fourier transform of the source data $\{(y_2)_j\}$ and the Fourier adjustment $\{(W_{1/2})_k\}$.

The following equations are applied to evaluate the errors $\{(\varepsilon_{2'})_j\}$ in the data $\{(y_{2'})_j\}$, from the given data $\{(\varepsilon_2)_j\}$ and $\{(W_{1/2})_k\}$:

$$(\varepsilon_{2'})_j^2 = N^{-1} \sum_k (Z_2^2)_k (W_{1/2}^2)_k \exp(-2\pi ikj/N), \quad (30)$$

$$(Z_2^2)_k = \sum_j (\varepsilon_2)_j^2 \exp(2\pi ikj/N), \quad (31)$$

$$(W_{1/2}^2)_k = \sum_j (w_{1/2})_j^2 \exp(2\pi ikj/N), \quad (32)$$

$$(w_{1/2})_j = N^{-1} \sum_k (W_{1/2})_k \exp(-2\pi ikj/N). \quad (33)$$

3. Application to diffraction data of ZnO powder

3.1. Experimental

Standard ZnO powder (NIST SRM674) was filled into the hollow of the flat-plate specimen holder of diameter 30 mm. The specimen was rotated about its surface normal at one revolution s^{-1} during the measurement.

The powder diffraction data were collected with the MDS on the beamline BL4B$_2$ at the Photon Factory in Tsukuba (Toraya *et al.*, 1996). Six detectors labelled No. 1 to No. 6 from lower to higher angles, are attached at intervals of 25° to the 2Θ axis. Each of the detectors is composed of Soller slits with divergence FWHM (full width at half-maximum) of 1.0°, a

Ge(111) crystal analyser, scintillation counter, pre-amplifier and pulse-height analyser (PHA; Rigaku 5320C1). The incident beam, monochromated at $\lambda = 1.206$ Å, was restricted to 1.0 mm in height and 10 mm in width by applying the entrance slits.

The angles of six crystal analysers were adjusted to maximize the signal from the attenuated direct beam, repeatedly changing the 2Θ angle at the interval of 25°, and carefully monitoring the values displayed by an encoder system (Heidenhain, RON-806) attached to the 2Θ axis.

The glancing angle of the incident beam at the sample face was set to 12.38°. The diffractometer was operated in 2Θ scan mode at a step interval of 0.005° with an integration time of 4 s. The 2Θ axis was scanned over -5.84 to 29.98°. Six segmented intensity data sets ranging -5.84 to 29.98°, 19.16 to 54.98°, 44.16 to 79.98°, 69.16 to 104.98°, 94.16 to 129.98° and 119.16 to 154.98° were collected with the No. 1 to No. 6 detectors, respectively.

The decay of the incident beam was monitored by measuring the intensity scattered by aluminium foil inserted in the incident beam path with another scintillation counter. The observed monitor intensity during the measurement is shown in Fig. 1. The dependence of the monitor intensity was fitted by

$$I = I_\infty + (I_0 - I_\infty) \exp(-t/T), \quad (34)$$

where t is the passed time, T the lifetime of the beam, and I_0 and I_∞ are the intensities expected for $t = 0$ and $t \to \infty$, respectively. The fitted values were used for correction of the change in the incident-beam intensity, because the deviations from the fit are almost fully assigned to the random errors predicted by counting statistics, as can be seen in Fig. 1.

3.2. Correction of counting losses

The counting losses caused by the finite response time of detection systems were modelled by an intermediately extended dead-time model (Ida & Iwata, 2005) given by
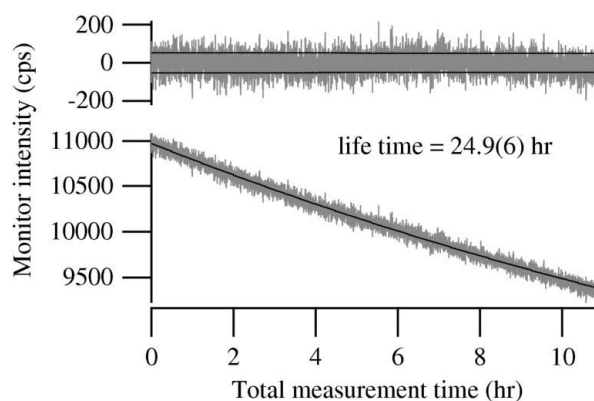

Figure 1
Intensity of the source X-ray measured with a monitor counter. The lower part shows the observed intensity (grey line) and exponential fit (black line). The upper part shows the errors predicted by counting statistics (black line) and the residuals of the fitting (grey line).

Table 1
The assumed parameters for counting losses.

τ is the dead-time and ρ is the degree of dead-time extension.

Detector	τ (μs)	ρ
No. 1	0.842 (5)	0.872 (15)
No. 2	1.185 (10)	0.68 (2)
No. 3	1.524 (8)	0.578 (9)
No. 4	1.188 (6)	0.682 (10)
No. 5	1.088 (6)	0.750 (13)
No. 6	1.327 (8)	0.639 (13)
Monitor	0.80 (12)	1 (fixed)

$$n = f(r; \tau, \rho)$$
$$= \begin{cases} t_2^{-1}[\exp(-r't_2) - \exp(-2r't_2)] & \text{for } t_2 \neq 0, \\ r' & \text{for } t_2 = 0, \end{cases} \quad (35)$$

with

$$r' = r/(1 + rt_1), \quad (36)$$

$$t_1 = \tau - 3t_2/2, \quad (37)$$

and

$$t_2 = (6\rho/13)^{1/2}\tau, \quad (38)$$

where n is the observed count rate, r is the true count rate, τ is the dead-time, and ρ is the degree of dead-time extension. The parameters for the counting losses experimentally determined by an improved foil method (Ida & Iwata, 2005) are summarized in Table 1. The errors that may be caused by the uncertainty of the assumed parameters were also taken into account in the analysis, in addition to the statistical uncertainty predicted by counting statistics.

The correction function as the inverse function of the above throughput function $f(r; \tau, \rho)$ is given by

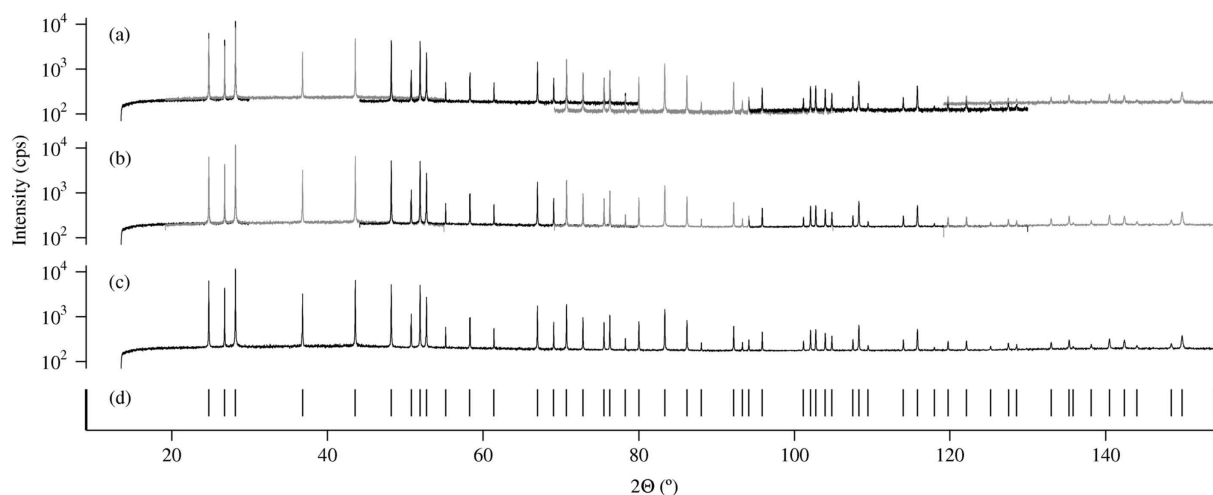$$r = f^{-1}(n; \tau, \rho) = r'/(1 - r't_1) \quad (39)$$

and

$$r' = \begin{cases} -t_2^{-1} \ln\{[1 + (1 - 4nt_2)^{1/2}]/2\} & \text{for } t_2 \neq 0, \\ n & \text{for } t_2 = 0, \end{cases} \quad (40)$$

where t_1 and t_2 are related to τ and ρ by equations (37) and (38).

3.3. Adjustment of segmented data

The experimental diffraction intensity profiles measured with the No. 1 to No. 6 detectors are shown in Fig. 2(a).

The segmented data measured with the No. 2 to No. 6 detectors are modified by the following procedures. First, the intensities in the second segment $\{(y_2)_j\}$ are modified to $\{(y_{2'})_j\}$ in order to adjust them to the intensities in the first segment $\{(y_1)_j\}$. Next, the intensities in the third segment $\{(y_3)_j\}$ are modified to $\{(y_{3'})_j\}$ to adjust them to the modified intensity data $\{(y_{2'})_j\}$ instead of the raw data $\{(y_2)_j\}$, for the purpose of creating a series of combined data by merging all the adjusted data segments. The fourth, fifth and sixth data segments are treated similarly.

3.3.1. Preliminary corrections for data segments. The correlations between the adjacent data sets in the overlapping range are analysed by the method described in §2.2.1. Fig. 3 shows the observed correlations and the results of fitting with a Lorentzian function.

Slight shifts of 0.0036, -0.0042, 0.0092, 0.0101 and 0.0101° have been found for the data measured with the No. 2 to No. 6 detectors, respectively. The shifts may have been caused by the errors in the initial adjustment of the angles of the analyser crystals.

The corrections for background determined by a least-squares optimization were $B = 79.3, 26.9, -50.9, -27.4$ and 52.9 counts s^{-1} for the No. 2 to No. 6 detectors, respectively. The linear fitting also gives the preliminary correction values for the sensitivities of the No. 2 to No. 6 detectors, estimated at $A = 0.695, 0.802, 0.913, 0.840$ and 0.660.

3.3.2. Fourier adjustment functions. Fig. 4 shows the experimental evaluations of the Fourier adjustment functions

Figure 2
Powder diffraction intensity profiles of ZnO measured with the MDS on BL4B$_2$ at the Photon Factory at the wavelength of 1.206 Å. (a) The raw, (b) adjusted and (c) combined intensities are shown. The data measured with No. 1, No. 3 and No. 5 detectors are shown as black lines, and the data measured with No. 2, No. 4 and No. 6 detectors are shown as grey lines in (a) and (b). The diffraction peak positions predicted for wurtzite ZnO are shown as vertical lines in (d).
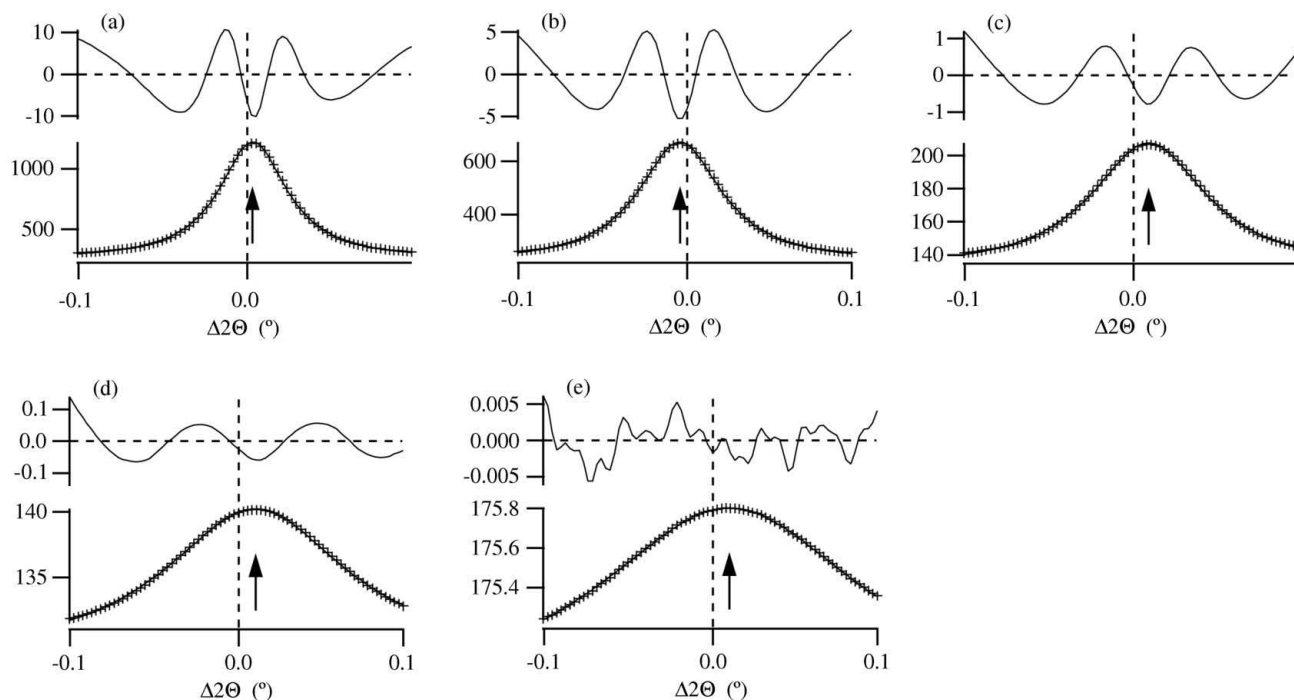
Figure 3
Correlations of the intensity data measured with the adjacent detectors: (a) No. 1 and No. 2, (b) No. 2′ and No. 3, (c) No. 3′ and No. 4, (d) No. 4′ and No. 5, (e) No. 5′ and No. 6. No. 2′ means the adjusted data measured with the No. 2 detector, and so on. The lower part of each panel shows the experimental correlations (crosses) and the optimized Lorentzian profile (solid line). The optimized peak positions are marked by vertical arrows. The upper part shows the difference between the experimental curve and the optimized Lorentzian.
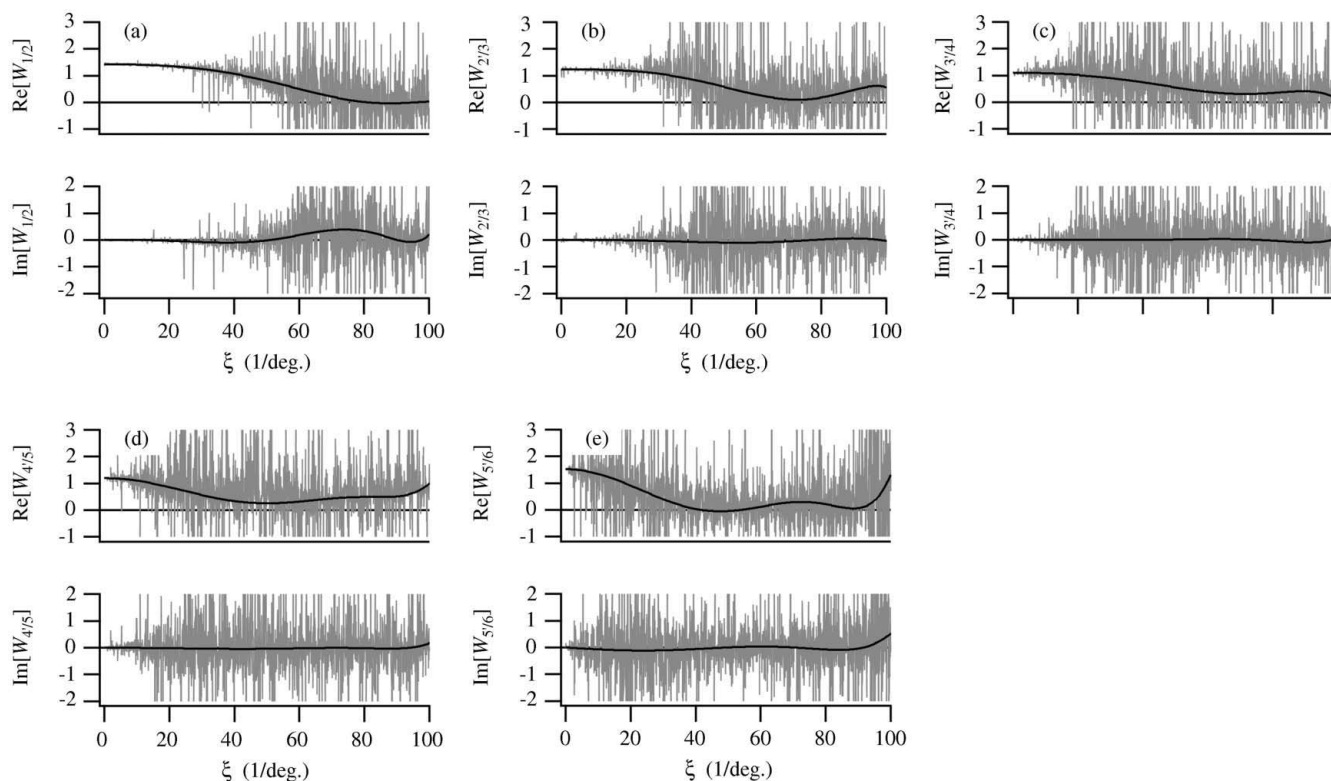

Figure 4
Fourier adjustments for the intensity data measured with the (a) No. 2, (b) No. 3, (c) No. 4, (d) No. 5 and (e) No. 6 detectors. The upper and lower parts of each panel show the real and imaginary parts of the Fourier correction functions. The experimental values are shown by grey lines, and the optimized polynomials are shown by black lines.

electronic reprint

as the ratios of the Fourier-transformed overlapping intensity data and the optimized polynomials described in §2.3. The polynomials with maximum order of 10 are used for the fitting, which are given by

$$f_{\text{poly,R}}(\xi) = \sum_{j=0}^{5} a_j \xi^{2j}, \tag{41}$$

and

$$f_{\text{poly,I}}(\xi) = \sum_{j=0}^{4} b_j \xi^{2j+1}, \tag{42}$$

where $\{a_j\}$ and $\{b_j\}$ are the fitting parameters.

Although the experimental evaluations of the Fourier adjustments are heavily affected by noisy structure, especially in the high-ξ regions, the behaviours near the origin are well reproduced by the optimized polynomials of ξ.

The sensitivities of the No. 2 to No. 6 detectors evaluated as the reciprocals of the Fourier adjustments at the origin $(1/a_0)$ are 0.697, 0.807, 0.914, 0.841 and 0.661 relative to that of the first detector. The values are consistent with the preliminary values evaluated in the preceding section.

The decrease in the real parts of the Fourier corrections on increasing ξ suggests that the data measured with the No. 1 detector are more broadened than those measured with other detectors, which may be caused by slightly lower resolution of the No. 1 detector.

3.3.3. Results of Fourier-based adjustment. The results of the Fourier-based adjustment are shown in Fig. 2(b). The angular dependence of the difference between the instrumental functions is neglected, because the observed difference is dominantly caused by slight misalignment of the analyser crystals, which does not directly affect the angular-dependent component of the instrumental function (Ida *et al.*, 2001). The adjusted data coincide well with the data in the adjacent segments. There are detectable deviations in the background intensities, while the main features of the peak profiles are only slightly deviated. Some data points located near the edges of the data segments show extraordinary values.

Fig. 2(c) shows a series of combined intensity data, obtained by merging the adjusted intensity data for each detector. The intensity values in the overlapping regions are evaluated as the weighted averages of the two intensity values by the following equation:

$$(y)_{j'} = (1 - \rho_{j'})(y_1)_{j'} + \rho_{j'}(y_{2'})_{j'}. \tag{43}$$

The weight $\rho_{j'}$ for the abscissa $x_{j'}$ is applied:

$$\rho_{j'} = \begin{cases} 2[(x_{j'} - x_{\text{L}})/(x_{\text{H}} - x_{\text{L}})]^2 \\ \quad \text{for } x_{\text{L}} \leq x_{j'} < (x_{\text{L}} + x_{\text{H}})/2, \\ 1 - 2[(x_{\text{H}} - x_{j'})/(x_{\text{H}} - x_{\text{L}})]^2 \\ \quad \text{for } (x_{\text{L}} + x_{\text{H}})/2 \leq x_{j'} < x_{\text{H}}, \end{cases} \tag{44}$$

where x_{L} and x_{H} are the lower and higher limits of the overlapping range, respectively. The extraordinary values observed near the edges of the data segments have automatically been removed by the above weighting scheme, where no contribution is assigned to the edge values.

3.4. Peak profile analysis

In order to examine the validity of the current method, the diffraction peak profiles measured with the No. 1 and No. 2 detectors, and the modified profiles calculated from the data measured with the No. 2 detector are analysed in this section.

To make the comparison easier, the preliminarily corrected data $\{(y_{2\text{p}})_j\}$ are further modified by

$$(y_{2''})_j = (y_{2\text{p}})_j/A, \tag{45}$$

where A is the preliminarily evaluated value for the sensitivity correction given in §3.3.1. The preliminarily corrected and scaled data set $\{(y_{2''})_j\}$ is labelled as No. 2$''$ data.

The function defined by the following equation is used as the model for the diffraction peak profiles:

$$p(x; b, S, x_0, \Gamma_{\text{S}}, \eta, \gamma_{\text{A}}) = b + Sf_{\text{ApV}}(x - x_0; \Gamma_{\text{S}}, \eta, \gamma_{\text{A}}), \tag{46}$$

where $f_{\text{ApV}}(x, \Gamma_{\text{S}}, \eta, \gamma_{\text{A}})$ is the asymmetrized pseudo-Voigt function defined by the convolution of the pseudo-Voigt function $f_{\text{pV}}(x; \Gamma_{\text{S}}, \eta)$ and a normalized asymmetric function $f_{\text{A}}(x; \gamma_{\text{A}})$,

$$f_{\text{ApV}}(x; \Gamma_{\text{S}}, \eta, \gamma_{\text{A}}) = f_{\text{pV}}(x; \Gamma_{\text{S}}, \eta) * f_{\text{A}}(x; \gamma_{\text{A}}). \tag{47}$$

The pseudo-Voigt function is defined by a linear combination of the Gaussian function $f_{\text{Gauss}}(x; w)$ and Lorentzian function $f_{\text{Lor}}(x; w)$ with the same full width at half-maximum, given by

$$f_{\text{pV}}(x; \Gamma_{\text{S}}, \eta) = (1 - \eta)f_{\text{Gauss}}[x; \Gamma_{\text{S}}/2(\ln 2)^{1/2}] + f_{\text{Lor}}(x; \Gamma_{\text{S}}/2), \tag{48}$$

where η is the shape parameter varying the sharpness of the peak profiles. The formula for the Gaussian function is given by

$$f_{\text{Gauss}}(x; w) = \pi^{-1/2}w^{-1}\exp(-x^2/w^2). \tag{49}$$

The definition of the Lorentzian function is given in equation (21). An asymmetric function of the following formula is applied here:

$$f_{\text{A}}(x; \gamma_{\text{A}}) = \begin{cases} |\gamma_{\text{A}}|^{-1}\exp(-x/\gamma_{\text{A}}) & \text{for } 0 \leq x/\gamma_{\text{A}}, \\ 0 & \text{for } x/\gamma_{\text{A}} < 0. \end{cases} \tag{50}$$

The constant background b, integrated intensity S, peak position x_0, FWHM of the symmetric component Γ_{S}, shape parameter of the pseudo-Voigt function ρ, and parameter for asymmetry γ_{A} are treated as profile parameters to be optimized.

Figs. 5–7 show the results for the raw 100, 002 and 101 reflection data measured with the No. 1 and No. 2 detectors, the preliminarily corrected and scaled profiles (No. 2$''$) and the final adjusted profiles (No. 2$'$) for the No. 2 detector. Other reflection peaks at higher diffraction angles showed relatively less significant difference in shape between adjacent detectors.

The fitting residuals are almost within the experimental errors for all the cases. It supports the validity of the error estimation described in §2.4 and also the errors estimated for the optimized parameters by the least-squares method. It also means that the currently applied sets of profile parameters sufficiently reproduce the experimental profiles; in other

Table 2
The optimized profile parameters for the 100 diffraction peak intensity data of ZnO powder measured with the No. 1 and No. 2 detectors.

The data listed under No. 2″ and No. 2′ are the preliminarily corrected and scaled values and final adjusted values calculated by the Fourier method, respectively. b is the constant background, S is the integrated intensity, $2\theta_0$ is the peak position, Γ_S and η are the full width at half-maximum (FWHM) and the shape parameter of the component pseudo-Voigt function, and γ_A is the asymmetry parameter.

	No. 1	No. 2	No. 2″	No. 2′
b	194 (3)	209 (3)	188 (4)	183 (3)
S	253.4 (10)	174.1 (9)	250.4 (13)	251.4 (8)
$2\theta_0$ (°)	24.7570 (3)	24.7547 (2)	24.7584 (2)	24.7573 (2)
Γ_S (°)	0.0261 (4)	0.0228 (4)	0.0228 (4)	0.0257 (3)
η	0.851 (11)	0.938 (16)	0.937 (16)	0.865 (10)
γ_A (°)	−0.0033 (4)	−0.0048 (3)	−0.0048 (3)	−0.0037 (3)

Table 3
The optimized profile parameters for the 002 diffraction peak intensity data of ZnO powder measured with the No. 1 and No. 2 detectors.

See Table 2 for definitions.

	No. 1	No. 2	No. 2″	No. 2′
b	193 (3)	214 (3)	194 (4)	193 (3)
S	155.6 (8)	108.6 (7)	156.2 (10)	156.4 (7)
$2\theta_0$ (°)	26.798 (3)	26.7977 (3)	26.8013 (3)	26.7999 (5)
Γ_S (°)	0.0261 (4)	0.0207 (5)	0.0207 (5)	0.0257 (3)
η	0.81 (2)	0.921 (19)	0.921 (19)	0.821 (13)
γ_A (°)	−0.001 (3)	−0.0038 (3)	−0.0038 (3)	−0.0024 (5)

Table 4
The optimized profile parameters for the 101 diffraction peak intensity data of ZnO powder measured with the No. 1 and No. 2 detectors.

See Table 2 for definitions.

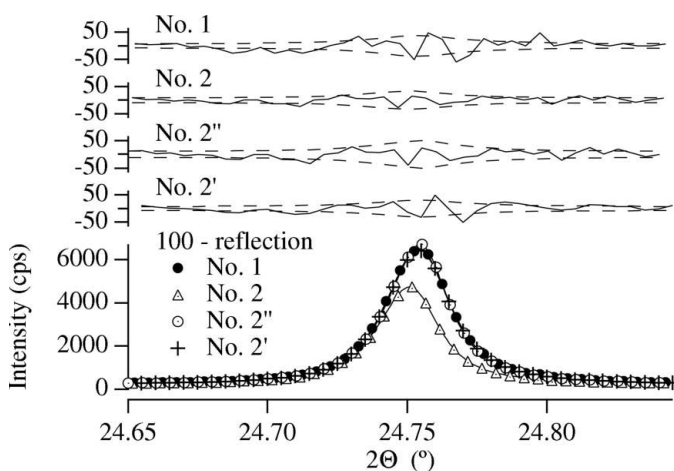|	No. 1	No. 2	No. 2″	No. 2′
b	182 (4)	209 (4)	189 (5)	183 (4)
S	477.3 (13)	331.7 (11)	477 (2)	478.2 (11)
$2\theta_0$ (°)	28.2069 (2)	28.2042 (2)	28.2078 (2)	28.2067 (2)
Γ_S (°)	0.0260 (3)	0.0237 (3)	0.0237 (3)	0.0265 (2)
η	0.884 (8)	0.936 (11)	0.935 (11)	0.866 (7)
γ_A (°)	−0.0036 (2)	−0.0046 (2)	−0.0046 (2)	−0.0035 (2)

Figure 5
The results of profile fitting for the 100 diffraction peak profiles of a ZnO powder sample measured with the No. 1 and No. 2 detectors. The lower part shows the raw, corrected and adjusted values of intensities as markers, and the fitted values as solid lines. The difference plots of the fitting are shown as solid lines in the upper part, accompanied by the experimental errors as broken lines. The raw intensity data are labelled No. 1 and No. 2, the preliminarily corrected and scaled values No. 2″, and the final adjusted values No. 2′. The broken lines labelled No. 2′ in the upper part were calculated by applying equations (30)–(33).
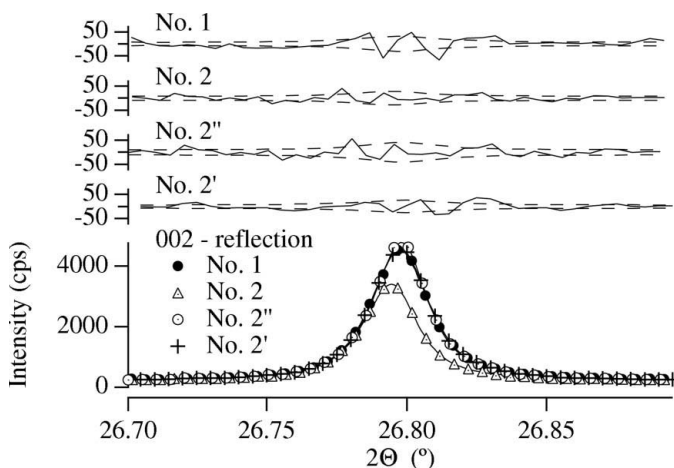

Figure 6
The results of profile fitting for the 002 diffraction peak profiles. See the caption of Fig. 5 for definitions.
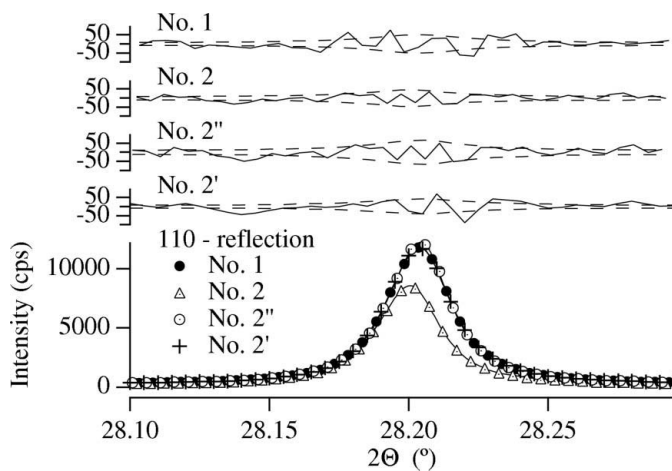

Figure 7
The results of profile fitting for the 101 diffraction peak profiles. See the caption of Fig. 5 for definitions.

words, no more information about the peak profiles could be extracted from the experimental data by adding any other parameters.

The optimized profile parameters are listed in Tables 2–4. The optimized values for the background b and integrated intensity S of the preliminarily corrected and scaled data (No. 2″) coincide well with the values estimated for the No. 1 profiles, but significant differences are found for the optimized values of x_0, Γ_S, η and γ_A. The smaller values of Γ_S in the No. 2 and No. 2″ profiles indicates that the peak profiles measured with the No. 2 detector is narrower than those measured with the No. 1 detector.

In contrast, all the optimized profile parameters for the No. 2′ data adjusted by the Fourier method coincide fairly well with the profile parameters for the No. 1 data within the

experimental errors, except that small differences are found in the background parameter of the 100 diffraction and η parameter of the 101 diffraction. This means that the current method has succeeded in adjusting the difference in width, asymmetry and sharpness of the peak profiles.

It should be noted that the procedures to adjust the segmented intensity data applied here do not require any diffraction peak profile fitting. It would be quite easy to automate the procedures for cases in which overlapping data regions exist, doubly measured with the adjacent detectors.

4. Conclusion

A Fourier method to connect segmented intensity data measured with a multiple-detector system has been developed. Not only the differences in background, sensitivity and shift in peak positions, but the differences in width, asymmetry and sharpness of the peak profiles measured with the adjacent detectors can be adjusted by the Fourier method with satisfactory precision.

References

Hodeau, J.-L., Bordet, P., Anne, M., Prat, A., Fitch, A. N., Dooryhée, E., Vaughan, G. & Freund, A. (1998). *Proc. SPIE*, **3448**, 356–361.
Ida, T., Hibino, H. & Toraya, H. (2001). *J. Appl. Cryst.* **34**, 144–151.
Ida, T. & Toraya, H. (2002). *J. Appl. Cryst.* **35**, 58–68.
Ida, T. & Iwata, Y. (2005). *J. Appl. Cryst.* **38**, 426–432.
Kaps, W. H., Ihringer, J., Prandl, W. & Schilling, M. (1999). *XVIIIth IUCr Congress Glasgow*, P13.01.016, S. 239–240.
Stokes, A. R. (1948). *Proc. Phys. Soc.* **61**, 382–391.
Toraya, H., Hibino, H. & Ohsumi, K. (1996). *J. Synchrotron Rad.* **3**, 75–83.